Chemical Engineering Science, Vol. 47, No. 8, pp. 1955–1961, 1992.
Printed in Great Britain.

0009–2509/92 $5.00 + 0.00

THE USE OF MICROELECTRODES FOR THE DETERMINATION OF FLOW REGIMES IN A TRICKLE-BED REACTOR

M. A. LATIFI, S. RODE, N. MIDOUX and A. STORCK
Laboratoire des Science du Génie Chimique, CNRS–ENSIC, BP 451, 1 rue Grandville, 54001 Nancy, France

(*Received* 28 *March* 1991; *accepted for publication* 23 *September* 1991)

Abstract—The utilization of microelectrodes in a non-conducting wall with subsequent signal analysis allowed the determination of flow regime transitions: trickling/pulsing, trickling/dispersed bubble and dispersed bubble/pulsing in a trickle-bed reactor by the analysis of the rate of fluctuation of the liquid–solid mass transfer coefficient (velocity gradient) variations as a function of liquid and gas flow rates.

1. INTRODUCTION

When gas and liquid flow cocurrently downward in a packed bed, different flow regimes are observed: trickling flow, pulsing flow, bubble flow and dispersed bubble flow. The transitions between these regimes depend on the superficial mass velocities, fluid properties and bed characteristics.

The control of these flow regimes is of great interest in the chemical industry. The flow regime is related to liquid distribution, pressure drop, hold-up, and heat and mass transfer. The choice of the particular regime depends on the nature of the reaction and the process conditions.

Several flow maps have been published for non-foaming systems in trickle-bed reactors (Weekman and Meyers, 1964; Charpentier *et al.*, 1972; Sato *et al.*, 1973; Charpentier and Favier, 1975; Midoux *et al.*, 1976; Specchia and Baldi, 1977; Talmor, 1977; Chou *et al.*, 1977; Gianetto *et al.*, 1978; Tosun, 1984).

The transitions between these different flow regimes are always determined by visual observations. They naturally depend on the observer. The idea is to use an objective and appropriate sensor which allows us to detect the different flow regimes and to identify their frontiers with great accuracy. In a recent study (Latifi *et al.*, 1989), we showed that the utilization of microelectrodes in a non-conducting wall allowed the determination of different flow regimes in a packed bed reactor with single-phase liquid flow.

The aim of the present work is to extend this technique of microelectrodes in a non-conducting wall to a packed bed reactor with downward cocurrent gas and liquid flow. The determination of flow regimes is carried out by the analysis of the rate of fluctuation of the liquid–solid mass transfer coefficient (velocity gradient) variations as a function of liquid and gas flow rates.

2. EXPERIMENTAL TECHNIQUE AND EQUIPMENT

2.1. *Description of the experimental rig*

Figure 1 is the schematic diagram of the equipment used in this study. The principal component is the glass column with an inside diameter of 5 cm packed with 5 mm glass spheres held fixed between two stainless steel grills. The packing height is 1.3 m and the overall bed porosity is 0.39.

Electrolyte is fed to the column by means of a centrifugal pump and the flow rate is measured with rotameters. At the outlet of the column, the liquid goes back to a storage tank where the temperature is maintained at 30°C. A compressed nitrogen gas from a cylinder was used as the gas phase. The pressure and the temperature are measured between the rotameters and the column.

The electrolyte solution is made up of a mixture of 10 mol/m^3 of hexacyanoferrate II ions and 1 mol/m^3 of hexacyanoferrate III ions in 500 mol/m^3 aqueous caustic soda solution. The measured physicochemical properties of fluids are: $\mu_G = 1.747 \times 10^{-5}$ Pa s, ρ_G ranging from 1.15 to 1.3 kg/m^3, $\rho_L = 1.018$ kg/m^3, $\mu_L = 0.9 \times 10^{-3}$ Pa s, $\sigma_L = 53 \times 10^{-3}$ N/m.

2.2. *Measurement method*

The local liquid–solid mass transfer coefficients K (over all microelectrodes) is deduced from the limiting current I_L, obtained by electrochemical reduction of hexacyanoferrate III ions, with the following classical relationship (Storck and Coeuret, 1984):

$$I_L = v_e F K A_e C_S \quad (1)$$

where $v_e F$ is the Faraday number involved in the reduction, A_e the electrode area and C_S the concentration of hexacyanoferrate III in the bulk of the solution.

2.3. *Measuring system and measuring circuit*

2.3.1. *The measuring system.* The measuring system consists of a network of 25 microelectrodes, each with a diameter of 250 μm flush-fitted in a 25 mm^2 surface on the inert wall of a plexiglass column element 10 cm high and inner diameter of 5 cm. The microelectrodes are set out on a 5 × 5 square array with a 1.187 mm spacing (cf. Fig. 2) (Latifi, 1988; Latifi *et al.*, 1989). Each of these 25 microelectrodes acts as a

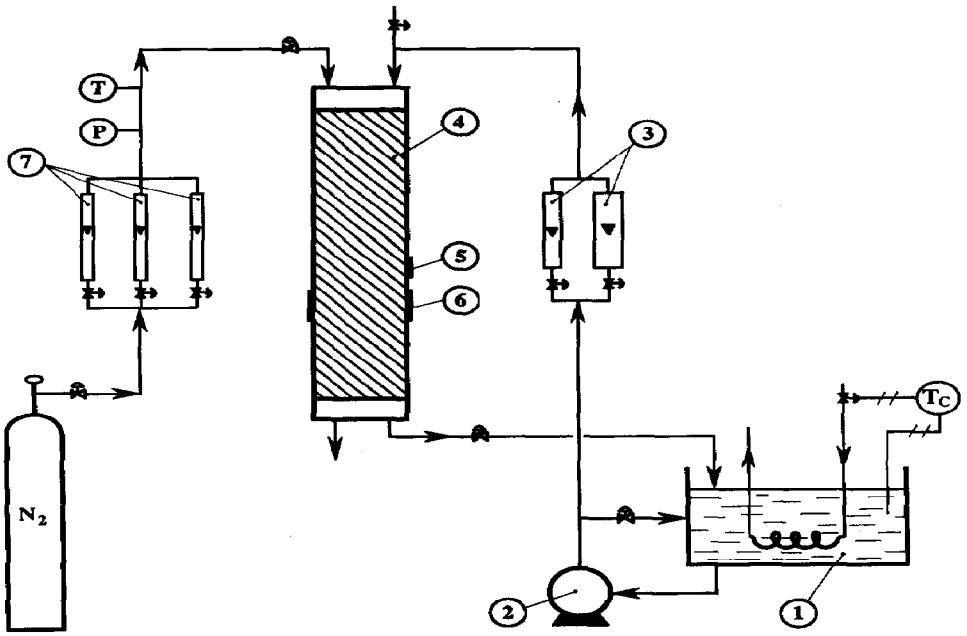

Fig. 1. Schematic view of the experimental equipment: (1) storage tank; (2) pump; (3) rotameters for the liquid; (4) column; (5) microelectrodes; (6) internally platinised nickel tube; (7) rotameter for the gas.

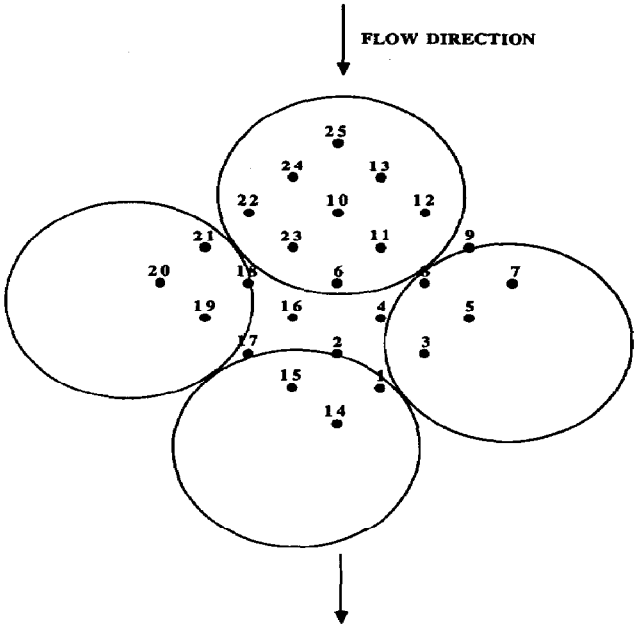

Fig. 2. Network of 25 microelectrodes.

working electrode. A nickel tube, platinised on the inside, 9 cm high and of the same diameter as the column, constitutes the counterelectrode.

2.3.2. *Measurement circuits.* The currents delivered by the microelectrodes are of very low intensity (of the order of a microampere) and are measurable using high resistances. They are converted into voltages and amplified to be accessible to standard data acquisition methods.

Figure 3 shows the measurement circuit. A battery is used to apply a voltage of -200 mV between the microelectrodes (cathode) and the platinised nickel tube (anode), which corresponds to the diffusional plateau of reduction of the hexacyanoferrate III ion and results in a current which varies with time. This current is converted into voltage using a resistance R ($10^4\ \Omega$) and is then amplified with a gain G (= 100) and cut-off frequency f_c (usually of the order of 1 kHz), which are both variable. The signal obtained in this way is digitized and stored on the hard disk of an

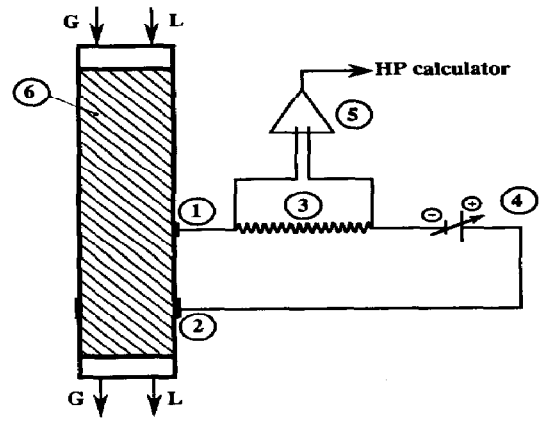

Fig. 3. Measurement circuit: (1) microelectrode; (2) counterelectrode; (3) resistance; (4) 4 V battery; (5) differential amplifier; (6) column.

HP 9000/360 calculator, and then treated by appropriate statistical techniques.

3. EXPERIMENTAL RESULTS AND INTERPRETATION

In the range of gas and liquid flows studied, four flow regimes are observed: trickle flow, bubble flow, dispersed or pseudo-homogeneous flow and pulsed flow. In this paper, we concentrate our interest in the limits of these different flow regimes by studying the fluctuation rate of the local mass transfer coefficient as a function of the gas and liquid flows.

3.1. *Measurement of the fluctuation rate of the local solid–liquid mass transfer coefficient*

The $K(t)$ signal can be decomposed in the following way:

$$K(t) = \bar{K} + k(t) \tag{2}$$

where $\bar{K}$ and $k(t)$ respectively represent the average value and the fluctuations of $K(t)$. The turbulent fluctuations $k(t)$ can be considered from the point of view of their quadratic averages $\bar{k}^2$ as the sum of the contributions of many different frequency bands. The power spectrum relative to the local mass transfer coefficient $K(t)$ is defined as (Max, 1985)

$$S_K^2(f) = F(f)F^*(f) \tag{3}$$

where $F(f)$ is the Fourier transform of the signal, i.e.

$$F(f) = \int_{-\infty}^{+\infty} K(t) \exp(-2\pi i f t)\, dt \tag{4}$$

and $F^*(f)$ is the conjugate of $F(f)$.

Thus we have

$$\bar{K} = [S_K^2(0)]^{1/2} \tag{5}$$

and

$$\bar{k}^2 = \int_{-\infty}^{+\infty} [S_K^2(f) - S_K^2(0)]\, df. \tag{6}$$

The fluctuation rate is then defined by the following relationship:

$$\sigma_K = (\bar{k}^2)^{1/2}/\bar{K}. \tag{7}$$

3.2. *Experimental results*

Before any measurement, the initially empty column is fed with a liquid flow of the order of 20 $kg\,m^{-2}\,s^{-1}$ without gas for about 5 min. The gas is then introduced by rapidly and progressively increasing the flow until the pulsed regime appears. This regime is maintained for about 1 min. This practice of starting with a high liquid flow, or flooding, is necessary to insure the reproducibility of the flow regimes and pressure losses. The initial high liquid flow pulsed regime gives a satisfactory wetting of the packing (Tosun, 1984).

Only those microelectrodes, which were constantly wetted in trickle flow, were used in this study. Changing the electrode changed the absolute value of the fluctuation rate, but the shape of the curves remained the same.

3.2.1. *Examples of signals obtained.* Figure 4 shows the type of time-scale signals obtained in each flow regime. In the trickle-flow regime, where the interactions between the gas and the liquid are weak, the signal fluctuates very slowly with time. In the strong-interaction regime (pulsed regime), the fluctuations are a great deal more rapid and of greater amplitude. The appearance of "pockets" in the signal corresponds to the passing of liquid plugs. In the dispersed regime, the signal characterizes the pseudo-homogeneous behaviour of the gas/liquid mixture. As opposed to these three stable-flow regimes, the transitional flow, characterized by low-frequency, high-energy fluctuations, is unstable.

3.2.2. *Analysis of the pulsed/trickle transition.* The study of this transition is based on the following procedure: The gas flow is fixed and starting from the dispersed-flow regime, the liquid flow is progressively reduced until the trickle-flow regime is obtained. Figure 5 gives an example of the curve obtained and shows the variation of the fluctuation rate σ_K as a function of the liquid flow for a fixed gas flow. It can be seen that this curve shows a maximum which corresponds to the change of flow regime and defines the coordinates L and G of the transition. The fact that σ_K passes through a maximum is explained by the high instability of the transitional flow. In a pulsed regime, the interactions become more important and σ_K goes down where L rises: the gas has a tendency to relatively cushion the fluctuations. These results, therefore, prove that the microelectrodes can detect the change of interaction between the gas and the liquid.

On the other hand, it does not seem possible to show the passing from the pulsed regime to the dispersed regime: at rising L the fluctuation rate goes steadily down from one regime to another.

3.2.3. *Transition: trickle/dispersed.* The procedure is the same as above. The gas flow is fixed and, starting from the dispersed regime, the liquid flow is progressively reduced until the trickle regime is obtained.

Figure 6 gives an example of the type of curve obtained (evolution of σ_K as a function of the liquid flow for a fixed gas flow). The curve also shows a maximum which corresponds to the change in flow regime and, in the same way as previously, defines the L and G coordinates of the transition. It is explained, as above, by the high instability of the transitional flow. In a dispersed or pseudo-homogeneous regime, the assimilation of the gas–liquid mixture to a viscoelastic homogeneous fluid would explain the decrease of σ_K when L increases, viscoelastic fluids being turbulence cushions with respect to Newtonian fluids. The slope characterizing the increase of σ_K as a function of L at the onset of transitional flow, starting from

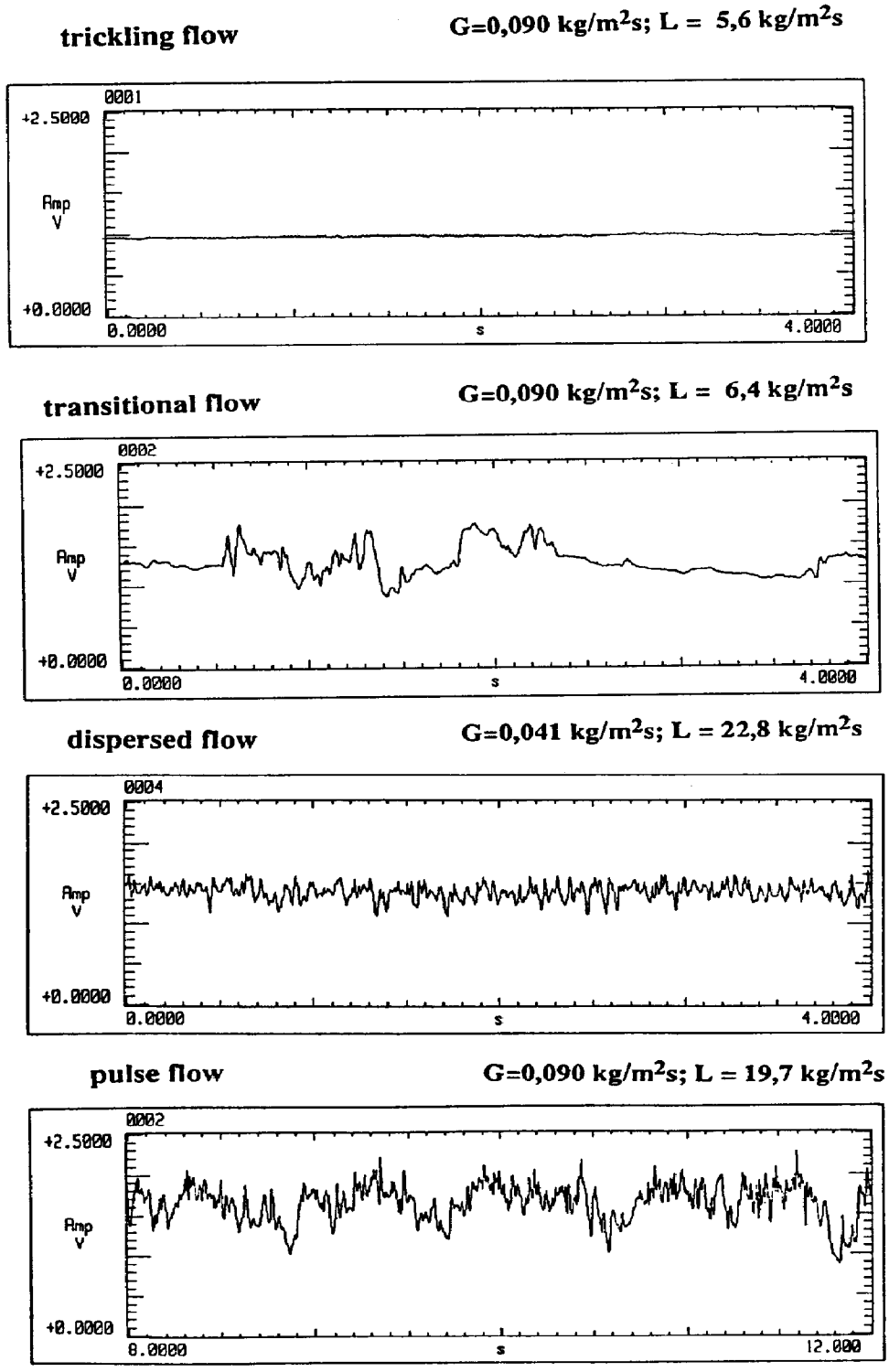

Fig. 4. Characteristic signal obtained for each flow regime.

trickle flow, is less high than in the previous case (cf. Fig. 4), since the change in interaction is less "sudden".

3.2.4. *Transition: dispersed/pulsed.* The procedure, used to study this transition, is the following. The liquid flow rate is fixed, and starting from the dispersed-flow regime, the gas flow rate is increased until the pulsed regime is obtained.

Figure 7 is given as an example and shows the variation of σ_K as a function of the gas flow for a fixed

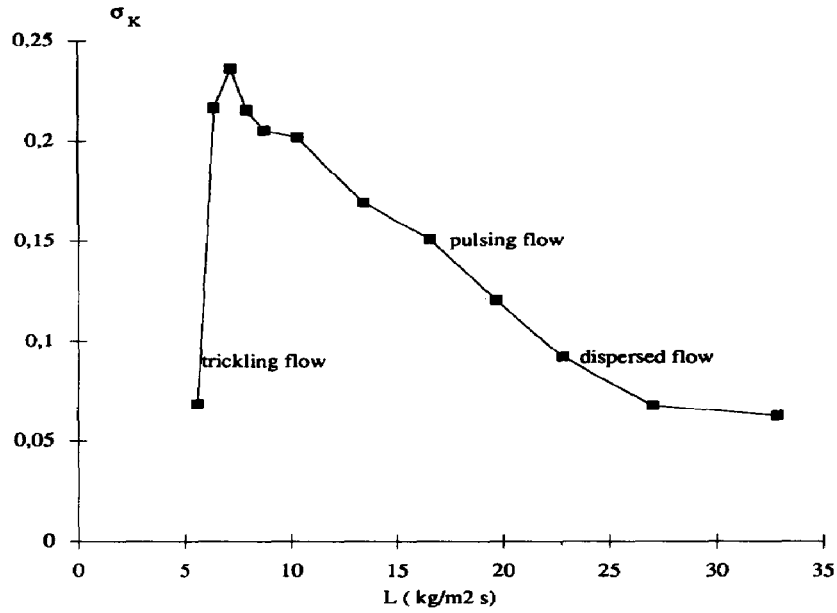

Fig. 5. Variation of the fluctuation rate as a function of L for $G = 0.095\ \mathrm{kg\,m^{-2}\,s^{-1}}$: trickle/pulsed transition.

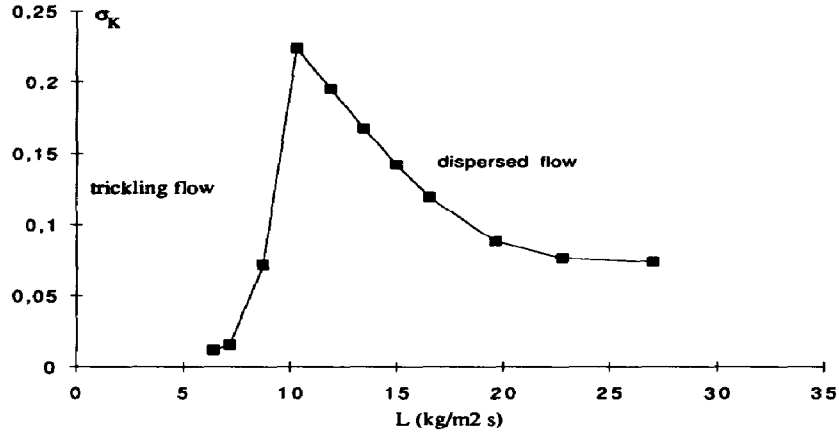

Fig. 6. Variation of the fluctuation rate as a function of L for $G = 0.015\ \mathrm{kg\,m^{-2}\,s^{-1}}$: trickle/dispersed transition.

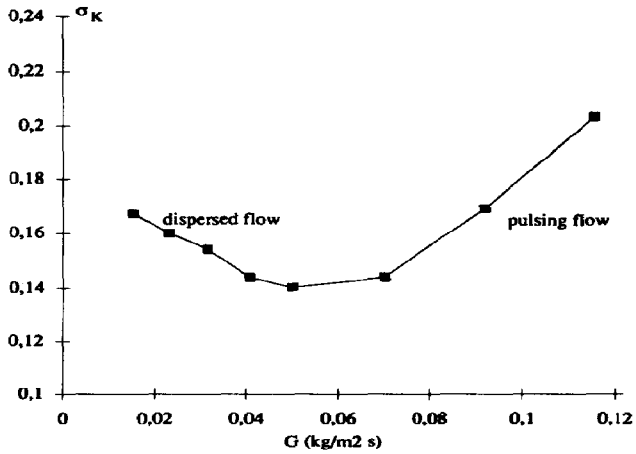

Fig. 7. Variation of the fluctuation rate as a function of G for $L = 13.4\ \mathrm{kg\,m^{-2}\,s^{-1}}$: dispersed/pulsed transition.

liquid flow rate. This curve has a minimum defining the coordinates L and G of the transition and is explained by the fact that, in a dispersed regime, the gas–liquid mixture behaves like a viscoelastic homogeneous fluid (σ_K decreases where G increases). In the pulsed regime, the conjugate effects of the passing of the liquid plugs and of the "rippling flow" below the plugs (where σ_K is very important) are the origin of a noticeable increase of σ_K with G.

3.3. *Comparison between microelectrode measurements and visual observations*

The transitional flow is visually detected by the observation of ripples as described by Tosun (Tosun, 1984), pulsing flow is noted when pulses traverse the entire length of the column.

Figure 8 shows, on the one hand, the transitions determined by visual observations and, on the other

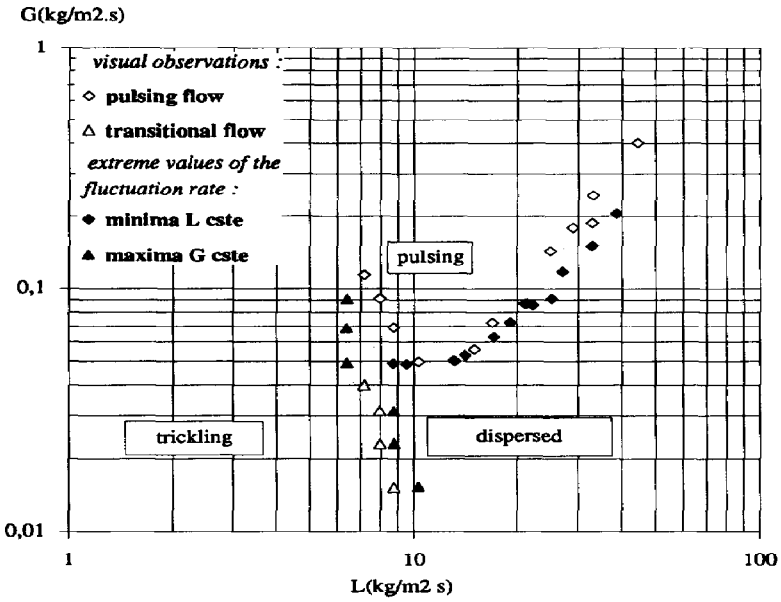

Fig. 8. Comparison between the visually observed limits and those determined by the microelectrode technique.

hand, those detected using the microelectrode technique; it clearly demonstrates that the two methods give similar results. For the trickle/pulsed transition, the visual frontier is slightly shifted relative to that determined by the microelectrodes. This is explained by the fact that the change of interaction between the gas and the liquid, accompanied by transitional flow, occurs before the onset of pulsing in the column.

Figure 9 gives the evolution of the fluctuation rate σ_K as function of gas flow. The liquid flow was held to $L = 9.3\,\mathrm{kg\,m^2\,s^{-1}}$ and, depending on gas flow rate, trickle and pulsed flow could be obtained. The gas flow has been progressively increased from the trickle-flow regime. We do not observe one, but two transitions, the first one (the maximum) corresponds to the transition between low and high interactions whereas the second one (the minimum) to the onset of pulsing.

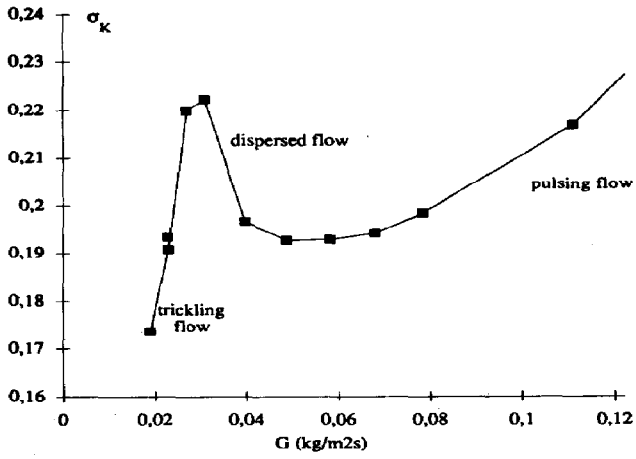

Fig. 9. Variations in the fluctuation rate as a function of G for $L = 9.3\,\mathrm{kg\,m^{-2}\,s^{-1}}$: trickle/dispersed and dispersed/pulsed transitions.

Finally, the results obtained by visual observations or with the help of the microelectrodes have been compared with those in the literature (Charpentier and Favier, 1975) in the form of the variations of $(L/G)\lambda\psi$ as a function of G/λ (cf. Fig. 10). Here again, the agreement is quite satisfactory.

4. CONCLUSION

The microelectrode in an inert wall technique associated with standard data treatment techniques constitutes a powerful tool for the determination of the transitions between the flow regimes in a trickle-bed reactor and has the advantage of not being observer dependent.

At the transition between the low-interaction regime, trickle-flow, and the high-interaction regimes, pulsed and dispersed flow, we always observed a transitional flow accompanied by a maximum value of the fluctuation rate σ_K. This transitional flow can develop, when L is increased either to dispersed or to pulsed flow, depending upon the gas flow rate.

However, this work demonstrates the limits of the technique:

(i) In the trickle-flow regime, measurements become difficult when the microelectrode used is not continuously irrigated.

(ii) This technique is not yet able to detect the transition between bubble and dispersed flows. The use of microelectrodes with smaller diameter should overcome this handicap.

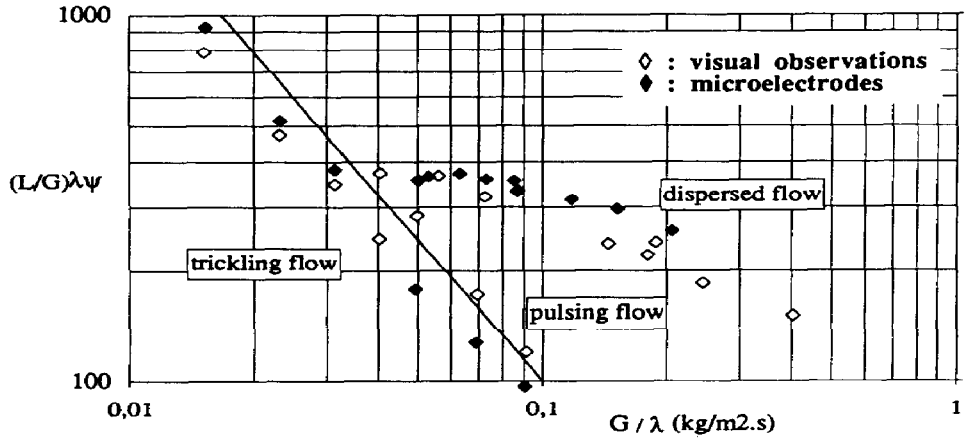

Fig. 10. Comparison between the visually observed limits and those obtained by microelectrodes with the results of Charpentier and Favier (1975).

This preliminary work using the simple analysis of the fluctuation rate of the local mass transfer coefficient at an inert wall, will be extended to a more complete analysis of the signals delivered by the microelectrodes (functions of auto- and inter-correlation; power density spectrum, etc.)

NOTATION

A_e electrode area, m^2
C_S concentration of electroactive species in the solution, mol/m^3
F Faraday constant = 96,500 C/equiv.
G superficial gas flow rate, $kg\ m^{-2}\ s^{-1}$
I_L limit diffusion current, A
K local liquid–solid mass transfer coefficient, m/s
$\bar{K}$ continuous component of the K coefficient, m/s
k fluctuating component of the K coefficient, m/s
L superficial liquid flow rate, $kg\ m^{-2}\ s^{-1}$

Greek letters

λ flow parameter ($= [(\rho_L/\rho_w)/(\rho_G/\rho_{air}]^{0.5}$)
μ dynamic viscosity, Pa s
ν_e number of electrons
ρ specific gravity, $kg\ m^{-3}$
σ superficial tension $N\ m^{-1}$
σ_K fluctuation rate of the local mass transfer coefficient
ψ flow parameter $[= (\sigma_w/\sigma_L)[(\mu_L/\mu_w)(\rho_L/\rho_w)^2]^{1/3}]$

Subscripts

G gas
L liquid
w water

REFERENCES

Charpentier, J. C., Bakos, M. and Le Goff, P., 1972, Traitement des produits pétroliers: regimes d'écoulement, chute de pression du gaz, taux de rétention et dispersion axiale du liquide pour des écoulements gaz–liquide à co-courant dans une colonne à garnissage. XII[ème] *journées de l'hydraulique*, Paris, Question IV, Rapport 10, 1–8.

Charpentier, J. C. and Favier, M., 1975, Some liquid hold-up experimental data in trickle-bed reactors for foaming and non-foaming hydrocarbons. *A.I.Ch.E. J.* **21**, 1213–1218.

Chou, T. S., Worley, F. L. and Luss, D., 1977, Transition to pulsed flow in mixed phase cocurrent downflow through a fixed bed. *Ind. Engng chem. Process Des. Dev.* **16**, 424–427.

Gianetto, A., Baldi, G., Specchia, V. and Sicardi, S., 1978, Hydrodynamics and solid–liquid contacting effectiveness in trickle-bed reactors. *A.I.Ch.E. J.* **24**, 1087–1104.

Latifi, M. A., 1988, Analyse globale et locale des phénomènes de transfert de matière liquid–solide dans un réacteur à lit fixe fonctionnant à co-courant vers le bas de gaz et de liquide. Thèse INPL, CNRS–ENSIC, Nancy, France.

Latifi, M. A., Midoux, N., Storck, A. and Jence, J. N., 1989, The use of micro-electrodes in the study of the flow regimes in a packed bed reactor with single phase liquid flow. *Chem. Engng Sci.* **44**, 2501–2508.

Max, J., 1985, *Méthodes et techniques de traitement du signal et applications aux mesures physiques*, 4[ème] Édition, tome 1. Masson, Paris.

Midoux, N., Favier, M. and Charpentier, J. C., 1976, Flow pattern, pressure loss and liquid holdup data in gas–liquid downflow packed beds with foaming and nonfoaming hydrocarbons. *J. Chem. Engng Japan* **9**, 350–356.

Sato, Y. T., Hirose, T., Takahashi, F., Toda, M. and Hashiguchi, Y., 1973, Flow pattern and pulsation properties of cocurrent gas–liquid downflow in packed-beds. *J. chem. Engng Japan* **6**, 315–319.

Specchia, V. and Baldi, G., 1977, Pressure drop and liquid holdup for two phase concurrent flow in packed beds. *Chem. Engng Sci.* **32**, 515–532.

Storck, A. and Coeuret, F., 1984, *Elements de génie electrochimique*. Tec. et Doc., Lavoisier, Paris.

Talmor, E., 1977, Two-phase flow through catalyst beds, *A.I.Ch.E. J.* **23**, 868–878.

Tosun, G., 1984, A study of cocurrent downflow of nonfoaming gas–liquid systems in a packed bed. 1. Flow regimes: search for a generalized flow map. *Ind. Engng Chem. Process Des. Dev.* **23**, 29–35.

Weekman, V. W. and Meyers, J. E., 1964, Fluid flow characteristics of concurrent gas–liquid flow in packed beds. *A.I.Ch.E. J.* **10**, 951–957.